VIP CO_2 Electroreduction Very Important Paper

International Edition: DOI: 10.1002/anie.201914977
German Edition: DOI: 10.1002/ange.201914977

Regulating the Coordination Environment of MOF-Templated Single-Atom Nickel Electrocatalysts for Boosting CO_2 Reduction

Yun-Nan Gong[+], Long Jiao[+], Yunyang Qian, Chun-Yang Pan, Lirong Zheng, Xuechao Cai, Bo Liu,* Shu-Hong Yu, and Hai-Long Jiang**

Abstract: *The general synthesis and control of the coordination environment of single-atom catalysts (SACs) remains a great challenge. Herein, a general host–guest cooperative protection strategy has been developed to construct SACs by introducing polypyrrole (PPy) into a bimetallic metal–organic framework. As an example, the introduction of Mg^{2+} in MgNi-MOF-74 extends the distance between adjacent Ni atoms; the PPy guests serve as N source to stabilize the isolated Ni atoms during pyrolysis. As a result, a series of single-atom Ni catalysts (named Ni_{SA}-N_x-C) with different N coordination numbers have been fabricated by controlling the pyrolysis temperature. Significantly, the Ni_{SA}-N_2-C catalyst, with the lowest N coordination number, achieves high CO Faradaic efficiency (98 %) and turnover frequency (1622 h^{-1}), far superior to those of Ni_{SA}-N_3-C and Ni_{SA}-N_4-C, in electrocatalytic CO_2 reduction. Theoretical calculations reveal that the low N coordination number of single-atom Ni sites in Ni_{SA}-N_2-C is favorable to the formation of COOH* intermediate and thus accounts for its superior activity.*

Single-atom catalysts (SACs), featured with metal atoms dispersed at atomic level, can achieve a maximal utilization of metal atoms and have demonstrated excellent catalytic performance for various reactions.[1] Combining the merits of both heterogeneous and homogenous catalysts, SACs have been regarded as a kind of unique heterogeneous catalysts to serve as an ideal model for the exploration of structure–property relationships during reaction processes.[2] The atomically dispersed metal atoms of SACs are stabilized by the support through coordination interaction to minimize their surface energy. Therefore, the local coordination environment usually plays a significant role for both catalytic activity and selectivity of SACs. Although much work has been devoted in this field, to our knowledge, accurate control over the coordination environment of SACs at an atomic level remains a great challenge and has been rarely investigated.[3]

Metal–organic frameworks (MOFs), a class of crystalline porous materials with well-defined structures and diverse compositions, not only exhibit great potentials for applications in diverse fields,[4] but also are promising precursors to produce desired materials for energy and catalysis.[5] Particularly, MOFs have recently emerged as an ideal platform for the construction of SACs, as the targeted metal atoms in MOFs can be rationally and spatially separated in an atomically dispersed form.[6] More specifically, because of the precisely designable and tailorable structures and components in MOFs, it is convenient to realize coordination environment regulation of SACs based on MOFs.[3b,c] While great progress has been achieved, the currently available strategies towards MOF-based SACs are limited to MOFs involving abundant N atoms, such as ZIFs[3b,c,6c,d,7] and porphyrinic MOFs.[8] Given that N atoms are not involved in most MOFs, it is highly desired to develop a more general approach for the construction of SACs based on all kinds of MOFs, including non-nitrogenous MOFs. As a representative, the MOF-74 isomers, constructed by different divalent M^{2+} ions (for example, Mg^{2+}, Ni^{2+}, Co^{2+}, etc.) and 2,5-dioxido-1,4-benzenedicarboxylate ligand,[9] can be synthesized under similar conditions. This approach enables metal tunability, making it easy to regulate and control the dispersion/concentration of different metal species in MOF-74 via a mixed-metal synthetic strategy.[10] In this respect, MOF-74

[*] Dr. Y.-N. Gong,[+] Dr. L. Jiao,[+] Y. Qian, Dr. X. Cai, Prof. Dr. B. Liu, Prof. Dr. S.-H. Yu, Prof. Dr. H.-L. Jiang
Hefei National Laboratory for Physical Sciences at the Microscale, CAS Key Laboratory of Soft Matter Chemistry, Collaborative Innovation Center of Suzhou Nano Science and Technology, Department of Chemistry, University of Science and Technology of China
Hefei, Anhui 230026 (P. R. China)
E-mail: liuchem@ustc.edu.cn
jianglab@ustc.edu.cn
Homepage: http://staff.ustc.edu.cn/~jianglab/
Dr. Y.-N. Gong[+]
Key Laboratory of Jiangxi University for Functional Material Chemistry, College of Chemistry & Chemical Engineering, Gannan Normal University, Ganzhou, Jiangxi 341000 (P. R. China)
Dr. Y.-N. Gong,[+] Prof. Dr. C.-Y. Pan
School of Light Industry and Chemical Engineering, Guangdong University of Technology, Guangzhou 510006 (P. R. China)
E-mail: panchuny@gdut.edu.cn
Dr. L. Zheng
Beijing Synchrotron Radiation Facility, Institute of High Energy Physics, Chinese Academy of Sciences
Beijing 100049 (P. R. China)
Dr. X. Cai
College of Chemistry and Molecular Engineering, Zhengzhou University, Zhengzhou 450001 (P. R. China)
Prof. Dr. H.-L. Jiang
State Key Laboratory of Structural Chemistry, Fujian Institute of Research on the Structure of Matter, Chinese Academy of Sciences, Fuzhou Fujian 350002 (P. R. China)
[+] These authors contributed equally to this work.
Supporting information and the ORCID identification number(s) for the author(s) of this article can be found under https://doi.org/10.1002/anie.201914977.

is a promising candidate to spatially separate particular metal atoms in its M-oxo chains and to create favorable premise for the accurate construction of SACs.

With the above in mind, a bimetallic MgNi-MOF-74 has been synthesized, in which a large amount of Mg^{2+} helps to realize spatial isolation of Ni^{2+} in M-oxo chains. Polypyrrole (PPy) molecules as the nitrogenous guests are filled into the 1D channels of the MOF, yielding a PPy@MgNi-MOF-74 composite. Upon pyrolysis, the N atoms of PPy are incorporated into the porous carbon derived from the composite and serve as anchor sites to stabilize the Ni atoms, after MgO removal by etching. By means of such a host–guest cooperative protection strategy, single-atom (SA) Ni implanted N-doped carbon catalysts (Ni_{SA}-N_x-C) with controlled Ni–N coordination number from 4 to 2 are obtained (Scheme 1). In addition, Fe and Co SACs can also be obtained following the same strategy, demonstrating its universality. The optimal catalyst, Ni_{SA}-N_2-C, exhibits much higher activity and selectivity than other catalysts for the electrochemical reduction of CO_2 to CO. DFT calculations unveil that the reduced coordination of Ni_{SA} by N atoms in Ni_{SA}-N_2-C favors the formation of a COOH* intermediate and thus improves the activity towards CO_2 reduction reaction (CO_2RR). To our knowledge, this is the first report on the fabrication of SACs from non-nitrogenous MOFs.

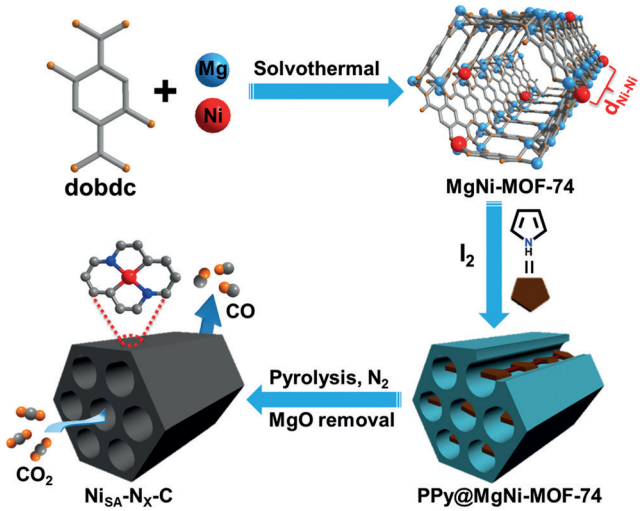

Scheme 1. Illustration showing the host–guest cooperative protection strategy for the fabrication of Ni_{SA}-N_x-C catalysts for electrocatalytic CO_2 reduction.

On the basis of the isomorphism of Mg-MOF-74 and Ni-MOF-74, the bimetallic MgNi-MOF-74 was first prepared via a one-pot solvothermal reaction (Figure S1 in the Supporting Information). Then, pyrrole (Py) monomer was introduced into the MOF channels followed by in situ oxidative polymerization in the presence of I_2, producing polypyrrole (PPy) confined in the MOF (denoted PPy@MgNi-MOF-74), during which the crystalline MOF structure can be retained (Figure S1). The solid-state UV/Vis absorption spectrum shows the characteristic PPy absorption band, confirming the incorporation of PPy in MgNi-MOF-74 (Figure S2).[11] The sharply reduced Brunauer–Emmett–Teller (BET) surface area (0.63 $m^2 g^{-1}$) compared with pristine MgNi-MOF-74 (931.6 $m^2 g^{-1}$) further approves the successful incorporation of PPy in the MOF channels (Figure S3). Upon pyrolysis at different temperatures in N_2 followed by MgO removal, PPy@MgNi-MOF-74 can be transformed to Ni-implanted N-doped porous carbons, namely Ni_{SA}-N_4-C, Ni_{SA}-N_3-C and Ni_{SA}-N_2-C, respectively, for the samples obtained at 600, 800 and 900 °C, according to their actual nitrogen ratio (roughly 4:3:2, Table S1). Inductively coupled plasma atomic emission spectroscopy (ICP-AES) analysis reveals similar Ni contents in all three samples ($\approx$0.9 wt %, Table S1).

Taking Ni_{SA}-N_2-C as a representative, its powder X-ray diffraction (XRD) pattern shows two broad peaks in the ranges of 20–30° and 40–45° corresponding to the (002) and (101) planes of carbon, whereas no characteristic peak assigned to Ni crystals is observed (Figure S4). The Raman spectrum of Ni_{SA}-N_2-C displays two peaks at 1357 and 1596 cm^{-1}, assignable to disordered (D band) and graphitic carbon (G band), respectively. The corresponding intensity ratio of I_D/I_G is calculated to be 0.91, indicating a moderate degree of graphitization (Figure S5). The powder XRD and Raman data for Ni_{SA}-N_4-C and Ni_{SA}-N_3-C present similar results to those of Ni_{SA}-N_2-C (Figures S4, S5). In addition, Ni_{SA}-N_2-C possesses a high surface area (280.8 $m^2 g^{-1}$), comparable to Ni_{SA}-N_4-C (178.3 $m^2 g^{-1}$) and Ni_{SA}-N_3-C (322.1 $m^2 g^{-1}$). The hysteresis loops present in the N_2 sorption curves of all Ni_{SA}-N_x-C suggest the existence of abundant mesopores, which would be beneficial for the mass transfer during the catalytic process (Figure S6).

A transmission electron microscopy (TEM) image presents the porous structure of Ni_{SA}-N_2-C. No Ni nanoparticles (NPs) can be found (Figure 1 a), in accordance with the above N_2 sorption and powder XRD results (Figures S4, S6). Aberration-corrected HAADF-STEM images clearly demonstrate the existence of isolated Ni atoms (Figure 1 b, S7). Energy dispersive spectroscopy (EDS) mapping reveals the homogeneous distribution of Ni, N and C in Ni_{SA}-N_2-C (Figure 1 c). To examine the existing situation of N and Ni elements, X-ray photoelectron spectroscopy (XPS) has been further conducted. The N 1s XPS spectra can be fitted to five

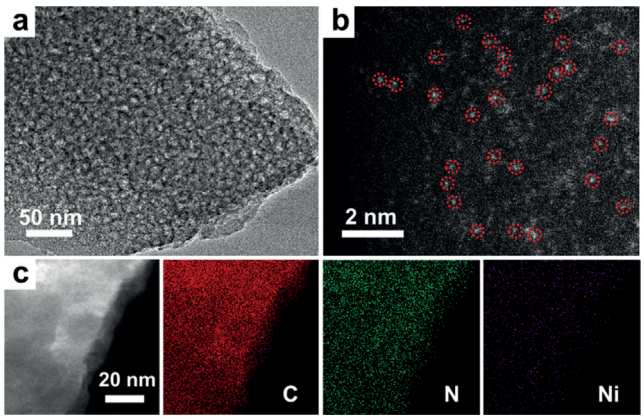

Figure 1. a) TEM and b) HAADF-STEM images of Ni_{SA}-N_2-C. c) EDS mapping of Ni, N and C elements in Ni_{SA}-N_2-C.

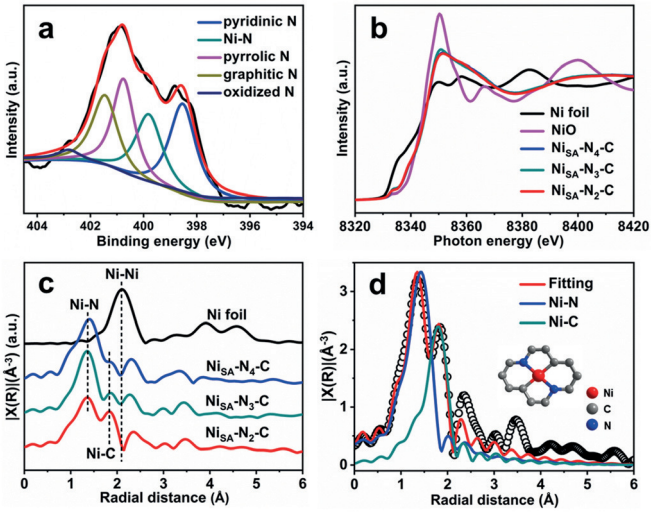

Figure 2. a) XPS spectrum of N 1s for Ni_{SA}-N_2-C. b) Normalized Ni K-edge XANES spectra and c) FT-EXAFS spectra of Ni_{SA}-N_x-C and Ni foil. d) EXAFS fitting and optimized model for Ni_{SA}-N_2-C.

characteristic peaks, including pyridinic N (398.5 eV), Ni-N (399.8 eV), pyrrolic N (400.7 eV), graphitic N (401.5 eV) and oxidized N (402.9 eV), respectively, supporting the successful N doping and the formation of Ni-N sites (Figure 2a).[12] The binding energy of Ni $2p_{3/2}$ in Ni_{SA}-N_2-C is located at 854.6 eV (Figure S8), which is in the range between metallic Ni^0 (853.0 eV) and Ni^{2+} (855.7 eV), suggesting a weakly oxidated state of the Ni species in Ni_{SA}-N_2-C.[3c]

To elucidate the electronic and microstructural information of Ni atoms in Ni_{SA}-N_x-C ($x = 2, 3, 4$), X-ray absorption spectroscopy (XAS) was utilized to determine their valence states and coordination environments.

From the Ni K-edge X-ray absorption near-edge structure (XANES) spectra, the absorption edge of the three samples are all located between those of Ni foil and NiO, manifesting the positive valence of Ni atom situated between Ni^0 and Ni^{2+}, in accordance with the XPS results (Figure 2b, Figure S8).[7a] In the Fourier transform-extended X-ray absorption fine structure (FT-EXAFS) spectra, all three samples exhibit dominant peaks corresponding to the Ni–N (≈1.36 Å) and Ni–C (≈1.87 Å) scattering paths. Importantly, the peak related to Ni–Ni bond in Ni foil (≈2.10 Å) is not observable in the profiles of Ni_{SA}-N_x-C ($x = 2, 3, 4$), verifying the formation of single Ni atoms in the samples (Figure 2c). To acquire more information on the chemical configuration, EXAFS fittings were performed (Figure 2d, Figure S9). The best fitting results reveal that, in addition to the 1 to 2 carbon atoms coordinated to each Ni atom, the Ni–N coordination numbers are 4.0, 3.4 and 2.0, respectively, for Ni_{SA}-N_4-C, Ni_{SA}-N_3-C and Ni_{SA}-N_2-C, which is in good agreement with the N ratios reflected by the elemental analysis (Tables S1 and S2). The results suggest that the introduction of abundant N source is crucial for stabilizing the single Ni atoms and avoiding their aggregation. Despite this, when the pyrolysis temperature increases to 1000 °C, Ni NPs (≈20 nm) can be clearly observed, demonstrating that 900 °C is the upper limit temperature for the formation of SA Ni catalysts (Figure S10). In addition, the increased Ni content (to 1.5-fold) in MgNi-MOF-74 also led to the formation of Ni NPs by pyrolysis at 900 °C, suggesting that the current Ni content in MgNi-MOF-74 is the optimal value (Figure S11).

For better comparison, PPy was also incorporated into monometallic Ni-MOF-74 followed by pyrolysis at 900 °C. The resulting material shows the existence of Ni NPs in the N-doped carbon (denoted as Ni_{NP}-N-C) (Figure S12). This illustrates the important role of Mg for extending the spatial separation of Ni atoms in the MOF skeleton. Direct pyrolysis of MgNi-MOF-74 without PPy leads to the formation of NiO NPs loaded on porous carbon (NiO_{NP}-C) (Figure S13), reflecting that the N atoms from PPy are of great significance for the stabilization of single Ni atoms. By means of this host (Mg)–guest (PPy) cooperative protection approach, Fe and Co SACs have been also achieved, validating the general applicability of this synthetic strategy (see details in the Supporting Information, Section 6, Figures S14–S21, Table S2), by which it is possible to extend the fabrication of SACs from the previous N-riched MOFs to all common MOFs.

Encouraged by the above results, electrocatalytic CO_2 reduction over Ni_{SA}-N_x-C has been investigated to evaluate the influence of the Ni–N coordination environment on catalytic performance. From the linear sweep voltammetry (LSV) curves, the current densities of Ni_{SA}-N_x-C ($x = 2, 3, 4$) in CO_2-saturated 0.5 M $KHCO_3$ are much higher than in N_2, indicating their activity in CO_2RR (Figures S22–S24). Remarkably, Ni_{SA}-N_2-C possesses a higher current density than Ni_{SA}-N_4-C and Ni_{SA}-N_3-C in CO_2-saturated 0.5 M $KHCO_3$, manifesting the best activity of Ni_{SA}-N_2-C for CO_2RR among all three single-atom Ni catalysts (Figure 3a). Furthermore, the Faradaic efficiencies (FE) for CO_2RR were examined in the potential range from −0.5 to −1.1 V (vs. RHE). As expected, Ni_{SA}-N_2-C affords a maximum CO FE of 98% at −0.8 V, which is the best FE among all measured SACs following a trend of Ni_{SA}-N_2-C > Ni_{SA}-N_3-C > Ni_{SA}-N_4-C (Figure 3b). The sums of FE for CO and H_2 are

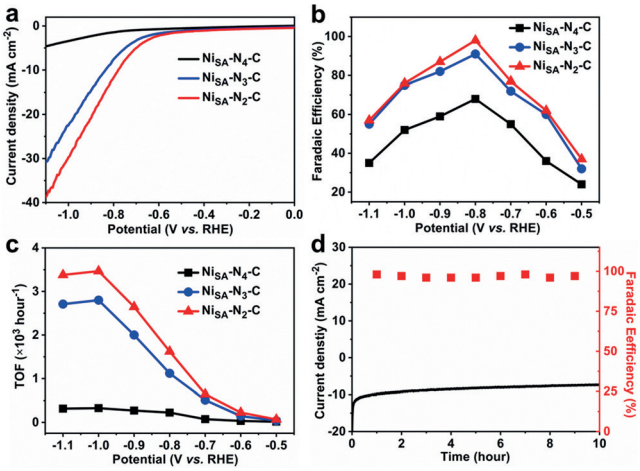

Figure 3. a) LSV curves in the CO_2-saturated 0.5 M $KHCO_3$ electrolyte, b) FEs of CO at different applied potentials, and c) the corresponding TOFs of CO production over Ni_{SA}-N_x-C. d) Stability of Ni_{SA}-N_2-C at −0.8 V during 10 h.

approximately 100% under all tested potentials for the three catalysts (Figure S25). No other carbonaceous products are generated, as detected by gas chromatographic (GC) analysis and ^{1}H NMR spectroscopy (Figure S26). Moreover, the TOF value for CO production of Ni_{SA}-N_2-C is 1622 h^{-1} at −0.8 V and reaches 3467 h^{-1} at −1.0 V, which are much higher than those of Ni_{SA}-N_4-C (225 h^{-1} at −0.8 V and 327 h^{-1} at −1.0 V) and Ni_{SA}-N_3-C (1120 h^{-1} at −0.8 V and 2800 h^{-1} at −1.0 V) (Figure 3c). The above results indicate that Ni_{SA}-N_2-C, featuring an Ni site coordinated by two nitrogen atoms, possesses the highest CO_2RR activity among the Ni_{SA}-N_x-C ($x = 2, 3, 4$) catalysts, unambiguously pointing out the vital role of the coordination environment of single-atom Ni for electrocatalytic CO_2RR. In contrast, Ni_{NP}-N-C featuring Ni NPs embedded in the catalyst shows a much lower current density, CO FE as well as TOF value than Ni_{SA}-N_2-C over the whole potential window, manifesting the superiority of single-atom Ni sites (Figures S27–S29). Moreover, the NiO_{NP}-C from MgNi-MOF-74 and metal-free N-doped carbon (N-C) derived from PPy@Mg-MOF-74 only give maximum CO FEs of 23% and 32%, respectively, far inferior to that of Ni_{SA}-N_2-C (Figure S30). All these results clearly suggest that the atomically dispersed Ni-N_2 sites in Ni_{SA}-N_2-C are the active sites for CO_2RR.

In view of the excellent performance of Ni_{SA}-N_2-C, electrochemical impedance spectroscopy (EIS) for Ni_{SA}-N_2-C exhibits the lowest charge-transfer resistance, providing the fastest charge-transfer process among all Ni_{SA}-N_x-C investigated (Figure S31). The Tafel slope of Ni_{SA}-N_2-C is calculated to be 208 mV/decade, smaller than that of Ni_{SA}-N_3-C (245 mV/decade) and Ni_{SA}-N_4-C (335 mV/decade), indicating favorable kinetics for CO_2RR of Ni_{SA}-N_2-C (Figure S32). In addition to the excellent activity and selectivity, Ni_{SA}-N_2-C presents nearly unchanged current density and FE for CO production even after electrolyzation for 10 h at −0.8 V, suggesting its long-term stability (Figure 3d).

Furthermore, DFT calculations were carried out to obtain insights on how the Ni coordination environment affects its activity. The reaction paths of CO_2RR to CO is generally a two-electron and two-proton transfer process (Figure 4a, Figure S33).[13] The Gibbs free-energy calculations along with the reaction paths of CO_2RR reveal that the formation of COOH* intermediates is the rate-determining step (RDS) for all the Ni_{SA}-N_x-C catalysts (Figure 4b). Obviously, the required free-energy change (ΔG) of RDS for Ni_{SA}-N_2-C is determined to be 1.42 eV, lower than that of Ni_{SA}-N_4-C (1.73 eV) and Ni_{SA}-N_3-C (1.45 eV). This implies that the formation of COOH* is easier on the Ni-N_2 sites in Ni_{SA}-N_2-C. In addition, Ni_{SA}-N_2-C also shows a much lower desorption energy of 0.47 eV for the formation of CO* than that of Ni_{SA}-N_4-C (1.09 eV) and Ni_{SA}-N_3-C (1.03 eV), suggesting the ease of CO* release from Ni_{SA}-N_2-C for CO production (Figure 4b). The results above reasonably explain the much higher CO_2RR efficiency of Ni_{SA}-N_2-C than Ni_{SA}-N_4-C and Ni_{SA}-N_3-C catalysts.

In summary, a host–guest cooperative protection strategy has been developed to construct SACs by in situ polymerization of Py in the 1D channels of bimetallic MgNi-MOF-74. During the pyrolysis, the Mg^{2+} ions in PPy@MgNi-MOF-74 help to realize the spatial separation of Ni atoms. PPy serves as the N source and protective "fence" to coordinate and prevent the aggregation of the separated Ni atoms. By simply controlling the pyrolysis temperature, the N coordination numbers of single Ni atoms can be well controlled and this is surprisingly critical to the performance of electrocatalytic CO_2 reduction. Specifically, the optimal Ni_{SA}-N_2-C, with the single-atom Ni coordinated by two nitrogens and two carbons, exhibits excellent activity and selectivity, far outperforming the counterpart catalysts featuring the Ni center coordinated by more N atoms, such as Ni_{SA}-N_3-C and Ni_{SA}-N_4-C. The lowest free-energy barrier for the rate-limiting step and very low CO* desorption energy of 0.47 eV of Ni_{SA}-N_2-C according to DFT calculations are assumed to be responsible for its superior catalytic performance among all Ni_{SA}-N_x-C. This work not only develops a novel and general strategy for the fabrication of SACs with tunable coordination environment, paving a way to the synthesis of SACs based on common MOFs, but also provides significant inspiration on boosting catalysis by controlling the metal coordination environment of SACs.

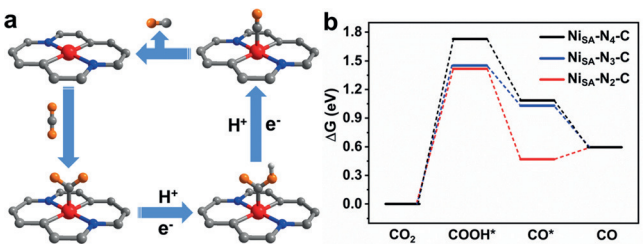

Figure 4. a) Proposed reaction paths for CO_2RR with Ni_{SA}-N_2-C as a model. b) Free-energy diagram of CO_2 reduction to CO over Ni_{SA}-N_x-C catalysts.

Acknowledgements

This work is supported by the NSFC (21725101, 21871244, 21521001, 21571167, 21671044), the China Postdoctoral Science Foundation (2018M633007, 2019TQ0298), the Fundamental Research Funds for the Central Universities (WK2060030029, WK2060190053), and the Fujian Institute of Innovation, CAS. We thank the 1W1B station for XAFS measurements at BSRF. The calculations were conducted at the Supercomputing Center of USTC.

Conflict of interest

The authors declare no conflict of interest.

Keywords: CO_2 electroreduction · coordination environment · metal–organic frameworks · single-atom catalysts

How to cite: *Angew. Chem. Int. Ed.* **2020**, *59*, 2705–2709
Angew. Chem. **2020**, *132*, 2727–2731

[1] a) X. Su, X.-F. Yang, Y. Huang, B. Liu, T. Zhang, *Acc. Chem. Res.* **2019**, *52*, 656; b) P. Liu, Y. Zhao, R. Qin, S. Mo, G. Chen, L. Gu, D. M. Chevrier, P. Zhang, Q. Guo, D. Zang, B. Wu, G. Fu, N. Zheng, *Science* **2016**, *352*, 797; c) H. Fei, J. Dong, Y. Feng, C. S. Allen, C. Wan, B. Volosskiy, M. Li, Z. Zhao, Y. Wang, H. Sun, P. An, W. Chen, Z. Guo, C. Lee, D. Chen, I. Shakir, M. Liu, T. Hu, Y. Li, A. I. Kirkland, X. Duan, Y. Huang, *Nat. Catal.* **2018**, *1*, 63; d) Y. Han, Z. Wang, R. Xu, W. Zhang, W. Chen, L. Zheng, J. Zhang, J. Luo, K. Wu, Y. Zhu, C. Chen, Q. Peng, Q. Liu, P. Hu, D. Wang, Y. Li, *Angew. Chem. Int. Ed.* **2018**, *57*, 11262; *Angew. Chem.* **2018**, *130*, 11432; e) J. Li, S. Chen, N. Yang, M. Deng, S. Ibraheem, J. Deng, J. Li, L. Li, Z. Wei, *Angew. Chem. Int. Ed.* **2019**, *58*, 7035; *Angew. Chem.* **2019**, *131*, 7109; f) T. Zheng, K. Jiang, H. Wang, *Adv. Mater.* **2018**, *30*, 1802066; g) X. Liu, Y. Jiao, Y. Zheng, M. Jaroniec, S.-Z. Qiao, *J. Am. Chem. Soc.* **2019**, *141*, 9664.

[2] a) L. Fan, P. F. Liu, X. Yan, L. Gu, Z. Z. Yang, H. G. Yang, S. Qiu, X. Yao, *Nat. Commun.* **2016**, *7*, 10667; b) J. Gu, C.-S. Hsu, L. Bai, H. M. Chen, X. Hu, *Science* **2019**, *364*, 1091; c) T. Möller, W. Ju, A. Bagger, X. Wang, F. Luo, T. N. Thanh, A. S. Varela, J. Rossmeisl, P. Strasser, *Energy Environ. Sci.* **2019**, *12*, 640; d) Y. J. Sa, S. O. Park, G. Y. Jung, T. J. Shin, H. Y. Jeong, S. K. Kwak, S. H. Joo, *ACS Catal.* **2019**, *9*, 83.

[3] a) W. Liu, L. Zhang, X. Liu, X. Liu, X. Yang, S. Miao, W. Wang, A. Wang, T. Zhang, *J. Am. Chem. Soc.* **2017**, *139*, 10790; b) X. Wang, Z. Chen, X. Zhao, T. Yao, W. Chen, R. You, C. Zhao, G. Wu, J. Wang, W. Huang, J. Yang, X. Hong, S. Wei, Y. Wu, Y. Li, *Angew. Chem. Int. Ed.* **2018**, *57*, 1944; *Angew. Chem.* **2018**, *130*, 1962; c) C. Yan, H. Li, Y. Ye, H. Wu, F. Cai, R. Si, J. Xiao, S. Miao, S. Xie, F. Yang, Y. Li, G. Wang, X. Bao, *Energy Environ. Sci.* **2018**, *11*, 1204; d) Y. Pan, Y. Chen, K. Wu, Z. Chen, S. Liu, X. Cao, W.-C. Cheong, T. Meng, J. Luo, L. Zheng, C. Liu, D. Wang, Q. Peng, J. Li, C. Chen, *Nat. Commun.* **2019**, *10*, 4290.

[4] a) H.-C. Zhou, S. Kitagawa, *Chem. Soc. Rev.* **2014**, *43*, 5415; b) M. Zhao, K. Yuan, Y. Wang, G. Li, J. Guo, L. Gu, W. Hu, H. Zhao, Z. Tang, *Nature* **2016**, *539*, 76; c) T. Islamoglu, S. Goswami, Z. Li, A. J. Howarth, O. K. Farha, J. T. Hupp, *Acc. Chem. Res.* **2017**, *50*, 805; d) Y.-B. Huang, J. Liang, X.-S. Wang, R. Cao, *Chem. Soc. Rev.* **2017**, *46*, 126; e) Y.-H. Luo, L.-Z. Dong, J. Liu, S.-L. Li, Y.-Q. Lan, *Coord. Chem. Rev.* **2019**, *390*, 86; f) R.-B. Lin, S. Xiang, H. Xing, W. Zhou, B. Chen, *Coord. Chem. Rev.* **2019**, *378*, 87; g) H. Yang, F. Peng, C. Dang, Y. Wang, D. Hu, X. Zhao, P. Feng, X. Bu, *J. Am. Chem. Soc.* **2019**, *141*, 9808; h) L. Jiao, J. Y. R. Seow, W. S. Skinner, Z. U. Wang, H.-L. Jiang, *Mater. Today* **2019**, *27*, 43; i) D. Li, H.-Q. Xu, L. Jiao, H.-L. Jiang, *EnergyChem* **2019**, *1*, 100005.

[5] a) S. Dang, Q.-L. Zhu, Q. Xu, *Nat. Rev. Mater.* **2017**, *3*, 17075; b) K. J. Lee, J. H. Lee, S. Jeoung, H. R. Moon, *Acc. Chem. Res.* **2017**, *50*, 2684; c) Y.-Z. Chen, R. Zhang, L. Jiao, H.-L. Jiang, *Coord. Chem. Rev.* **2018**, *362*, 1; d) X. Wang, L. Yu, B. Y. Guan, S. Song, X. W. Lou, *Adv. Mater.* **2018**, *30*, 1801211; e) B. Zhu, D. Xia, R. Zou, *Coord. Chem. Rev.* **2018**, *376*, 430; f) G. Anandhababu, Y. Huang, D. D. Babu, M. Wu, Y. Wang, *Adv. Funct. Mater.* **2018**, *28*, 1706120.

[6] a) Y. Zheng, S.-Z. Qiao, *Natl. Sci. Rev.* **2018**, *5*, 626; b) L. Jiao, H.-L. Jiang, *Chem* **2019**, *5*, 786; c) E. Luo, H. Zhang, X. Wang, L. Gao, L. Gong, T. Zhao, Z. Jin, J. Ge, Z. Jiang, C. Liu, W. Xing, *Angew. Chem. Int. Ed.* **2019**, *58*, 12469; *Angew. Chem.* **2019**, *131*, 12599; d) H. Zhang, S. Hwang, M. Wang, Z. Feng, S. Karakalos, L. Luo, Z. Qiao, X. Xie, C. Wang, D. Su, Y. Shao, G. Wu, *J. Am. Chem. Soc.* **2017**, *139*, 14143; e) M. Zhang, Q. Dai, H. Zheng, M. Chen, L. Dai, *Adv. Mater.* **2018**, *30*, 1705431.

[7] a) C. Zhao, X. Dai, T. Yao, W. Chen, X. Wang, J. Wang, J. Yang, S. Wei, Y. Wu, Y. Li, *J. Am. Chem. Soc.* **2017**, *139*, 8078; b) P. Lu, Y. Yang, J. Yao, M. Wang, S. Dipazir, M. Yuan, J. Zhang, X. Wang, Z. Xie, G. Zhang, *Appl. Catal. B: Environ.* **2019**, *241*, 113.

[8] a) T. He, S. Chen, B. Ni, Y. Gong, Z. Wu, L. Song, L. Gu, W. Hu, X. Wang, *Angew. Chem. Int. Ed.* **2018**, *57*, 3493; *Angew. Chem.* **2018**, *130*, 3551; b) L. Jiao, G. Wan, R. Zhang, H. Zhou, S. Yu, H.-L. Jiang, *Angew. Chem. Int. Ed.* **2018**, *57*, 8525; *Angew. Chem.* **2018**, *130*, 8661; c) X. Fang, Q. Shang, Y. Wang, L. Jiao, T. Yao, Y. Li, Q. Zhang, Y. Luo, H.-L. Jiang, *Adv. Mater.* **2018**, *30*, 1705112; d) O. Zuo, T. Liu, C. Chen, Y. Ji, X. Gong, Y. Mai, Y. Zhou, *Angew. Chem. Int. Ed.* **2019**, *58*, 10198; *Angew. Chem.* **2019**, *131*, 10304.

[9] a) N. L. Rosi, J. Kim, M. Eddaoudi, B. Chen, M. O'Keeffe, O. M. Yaghi, *J. Am. Chem. Soc.* **2005**, *127*, 1504; b) S. R. Caskey, A. G. Wong-Foy, A. J. Matzger, *J. Am. Chem. Soc.* **2008**, *130*, 10870.

[10] a) Y. Jiao, C. R. Morelock, N. C. Burtch, W. P. Mounfield, J. T. Hungerford, K. S. Walton, *Ind. Eng. Chem. Res.* **2015**, *54*, 12408; b) M. Y. Masoomi, A. Morsali, A. Dhakshinamoorthy, H. Garcia, *Angew. Chem. Int. Ed.* **2019**, *58*, 15188; *Angew. Chem.* **2019**, *131*, 15330; c) Y.-Z. Chen, C. Wang, Z.-Y. Wu, Y. Xiong, Q. Xu, S.-H. Yu, H.-L. Jiang, *Adv. Mater.* **2015**, *27*, 5010.

[11] B. Dhara, S. S. Nagarkar, J. Kumar, V. Kumar, P. K. Jha, S. K. Ghosh, S. Nair, N. Ballav, *J. Phys. Chem. Lett.* **2016**, *7*, 2945.

[12] H. B. Yang, S. Hung, S. Liu, K. Yuan, S. Miao, L. Zhang, X. Huang, H.-Y. Wang, W. Cai, R. Chen, J. Gao, X. Yang, W. Chen, Y. Huang, H. M. Chen, C. M. Li , T. Zhang, B. Liu, *Nat. Energy* **2018**, *3*, 140.

[13] a) Y. Zheng, A. Vasileff, X. Zhou, Y. Jiao, M. Jaroniec, S.-Z. Qiao, *J. Am. Chem. Soc.* **2019**, *141*, 7646; b) A. Vasileff, X. Zhi, C. Xu, L. Ge, Y. Jiao, Y. Zheng, S.-Z. Qiao, *ACS Catal.* **2019**, *9*, 9411; c) P. Chen, Y. Jiao, Y.-H. Zhu, S.-M. Chen, L. Song, M. Jaroniec, Y. Zheng, S.-Z. Qiao, *J. Mater. Chem. A* **2019**, *7*, 7675.

Manuscript received: November 24, 2019
Revised manuscript received: December 9, 2019
Accepted manuscript online: December 10, 2019
Version of record online: January 9, 2020

